

Magnetoelectric coupling tuned by competing anisotropies in $\text{Mn}_{1-x}\text{Ni}_x\text{TiO}_3$

Songxue Chi,¹ Feng Ye,^{1,2} H. D. Zhou,^{3,4} E. S. Choi,⁴ J. Hwang,⁴ Huibo Cao,¹ and Jaime A. Fernandez-Baca^{1,3}

¹Quantum Condensed Matter Division, Oak Ridge National Laboratory, Oak Ridge, Tennessee 37831, USA

²Department of Physics and Astronomy, University of Kentucky, Lexington, Kentucky 40506, USA

³Department of Physics and Astronomy, University of Tennessee, Knoxville, Tennessee 37996-1200, USA

⁴National High Magnetic Field Laboratory, Florida State University, Tallahassee, FL 32310-3706, USA

(Dated: February 29, 2024)

A flop of electric polarization from $P\parallel c$ (P_c) to $P\parallel a$ (P_a) is observed in MnTiO_3 as a spin flop transition is triggered by a c -axis magnetic field, $H_{\parallel c}=7$ T. The critical magnetic field $H_{\parallel c}$ for P_a is significantly reduced in $\text{Mn}_{1-x}\text{Ni}_x\text{TiO}_3$ ($x=0.33$). P_a and P_c have been observed with both $H_{\parallel c}$ and $H_{\parallel a}$. Neutron diffraction measurements revealed similar magnetic arrangements for the two compositions where the ordered spins couple antiferromagnetically with their nearest intra- and inter-planar neighbors. In the $x=0.33$ system, the uniaxial and planar anisotropies of Mn^{2+} and Ni^{2+} compete and give rise to a spin reorientation transition at T_R . A magnetic field, $H_{\parallel c}$, aligns the spins along c for $T_R < T < T_N$. The rotation of the collinear spins away from the c -axis for $T < T_R$ alters the magnetic point symmetry and gives rise to a new ME susceptibility tensor form. Such linear ME response provides satisfactory explanation for the behavior of the field-induced electric polarization in both compositions. As the Ni content increases to $x=0.5$ and 0.68 , the ME effect disappears as a new magnetic phase emerges.

PACS numbers: 78.70.Nx, 61.05.fm, 74.70.-b, 75.30.Fv

I. INTRODUCTION

The multiferroics that show strong magnetoelectric (ME) effect are among the most sought-after materials due to their multi-functionality of inducing polarization with magnetic field or magnetization with electric field.¹⁻⁶ The linear ME effect occurs in a crystal when the term $-\alpha_{ij}E_iH_j$ in the expansion of its Gibbs free energy $F(E, H)$ is nonzero. Here α is a second rank tensor which changes sign under space or time inversion, but is invariant when the occurrences of the two inversions are simultaneous.^{7,8} The magnetic symmetries that meet such conditions are allowed to have linear ME response. Therefore in exploring magnetoelectrics among materials with long range magnetic order, symmetry analysis serves as a reliable guide.⁹⁻¹¹ Such predictability can be obscured when extra microscopic complications, such as magnetic anisotropy, spin frustration and spin-lattice coupling, have been introduced. However, these extra variables sometimes help to increase the magnitude of α ¹¹⁻¹³ or even give rise to new ME coupling mechanisms.¹⁴⁻¹⁶

$\text{Mn}_{1-x}\text{Ni}_x\text{TiO}_3$ is such a system where more than one ME mechanism has emerged. MnTiO_3 and NiTiO_3 have the same ilmenite structure (Fig. 1)¹⁷ but different spin arrangements and easy axes,¹⁸ which compete in the mixed compounds. Also competing are the energy loss from single ion anisotropy and that from the frustration of the exchange interactions.¹⁹ Various new magnetic phases including spin glass (SG) phase emerge as a result, forming a rather complex phase diagram.¹⁹⁻²¹ While the linear ME effect was observed in MnTiO_3 as its magnetic symmetry permits,²² a new ME response is induced by the toroidal moments in the SG state of the

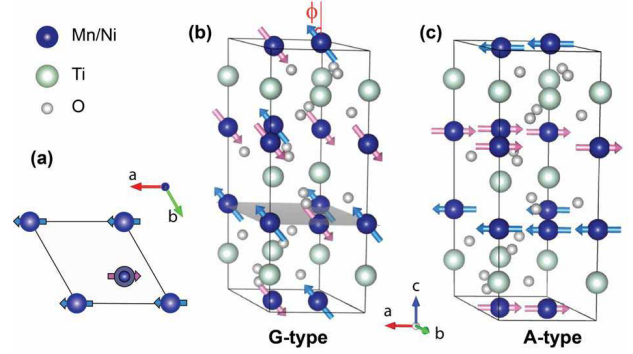


FIG. 1: (Color online) Primitive cells of the hexagonal lattice of the compounds $\text{Mn}_{1-x}\text{Ni}_x\text{TiO}_3$. (a) The top view of the hexagon of cations with respect to the rhombic cross section as shaded in (b). Note the vacant octahedral site and a cation displacement from the ab -plane. Two types of magnetic structures, G-type with real spin directions unspecified and A-type, are shown in (b) for Mn-rich compounds and (c) for the Ni-rich compounds. ϕ in (b) is the angle between the spins and the hexagonal c -axis.

mixed compounds.²³ On both sides of the SG phase, the unexplored spin flop transitions, short range magnetic correlations and the Ti^{4+} ions with empty $3d$ shells,^{24,25} are all potential hosts of yet another novel ME mechanism. Although the magnetic structures of the end-member compounds have been studied,¹⁸ the details of the magnetic evolution in the mixed compounds and its effect on the electric polarization are still lacking. This report presents a systematic investigation of the ME effects and the magnetic orders in $\text{Mn}_{1-x}\text{Ni}_x\text{TiO}_3$. New

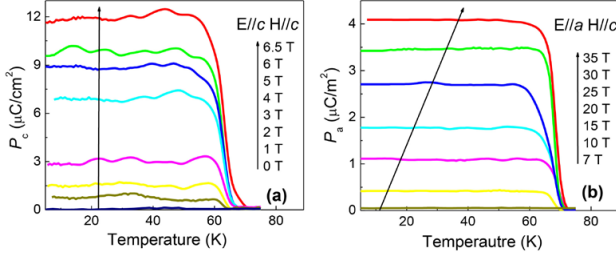


FIG. 2: (Color online) Temperature dependence of the electric polarization P of MnTiO_3 at various magnetic fields measured with $H \parallel c$ and (a) $E \parallel c$, and (b) $E \parallel a$. The temperature dependence of P for the $x=0.33$ compound with $H \parallel c$ and (c) $E \parallel c$, and (d) $E \parallel a$.

components of the ME tensor and an anomaly in their temperature dependence under a low magnetic field have been observed. Neutron diffraction measurement on the $x=0.33$ compound under an applied magnetic field reveals the effect of the field on the spin orientation and therefore, on the nature of the new ME coupling. Details of the magnetic orders in 4 typical compositions and corrections to the phase diagram are reported.

II. EXPERIMENTAL

Single crystals of $\text{Mn}_{1-x}\text{Ni}_x\text{TiO}_3$ ($x=0, 0.33, 0.50$ and 0.68) were grown by the traveling-solvent floating zone technique. For electric polarization measurements, silver epoxy was pasted on the crystals cut into thin plates. The pyroelectric current was measured using a Keithley 6517A electrometer on warming after poling the crystal in an electric field of 800 kV/m while cooling down from above T_N . The spontaneous polarization was obtained by integration of the pyroelectric current with respect to time. The single crystal neutron diffraction measurements were carried out at the High Flux Isotope Reactor of the Oak Ridge National Laboratory. The HB-2C Wide Angle Neutron Diffractometer (WAND) with wavelength of 1.482 Å was used for reciprocal space and diffuse scattering surveys. The collections of reflections for structural determination were carried out at HB-3A four circle diffractometer where the wavelength of 1.542 Å was chosen. An assembly of permanent magnets that provides 0.7 Tesla at the sample position was employed in the magnetic field measurement on HB-3A. Closed-cycle refrigerators were used on both diffractometers. The Rietveld refinements on the crystal and magnetic structures were conducted using the FullProf Suite.²⁶

III. RESULTS

A. Pyroelectric measurements under magnetic field

The ME effect was observed in $x=0$ and 0.33 . In both cases the pyroelectric current anomaly signaling the onset of polarization appears only when finite magnetic field

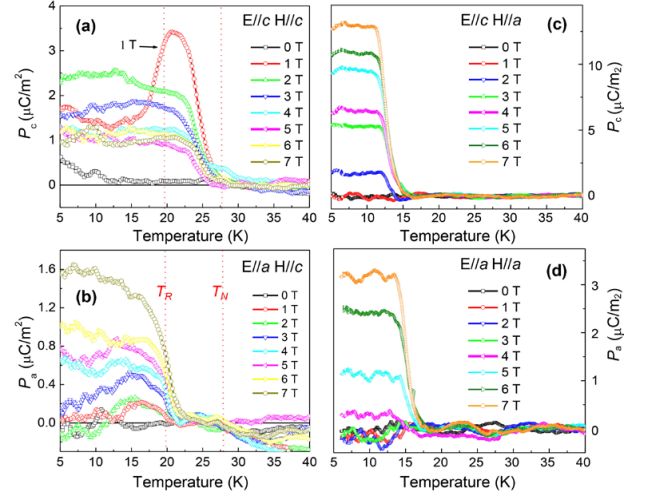


FIG. 3: (Color online) Temperature dependence of the electric polarization P of $\text{Mn}_{0.67}\text{Ni}_{0.33}\text{TiO}_3$ at various magnetic fields measured with $H \parallel c$ and (a) $E \parallel c$, and (b) $E \parallel a$. The temperature dependence of P for the $x=0.33$ compound with $H \parallel a$ and (c) $E \parallel c$, and (d) $E \parallel a$. The dotted red lines mark the Néel temperature and the onset temperature of the spin rotation under the magnetic field of 0.7 T.

is applied along c . Fig. 2 shows the temperature dependence of the spontaneous polarization (P) under various magnetic fields for the $x=0$ sample. The previous study²² only reported the observation of P_c in this compound. As shown in Fig.2(a), P_c increases monotonically with increasing field until $H_{\parallel c}=6.5$ T, then starts to decrease quickly and disappears above 7 T. The maximum value of P_c is about $12 \mu\text{C}/\text{m}$, which is consistent with ref²². The intensity of P_a , on the other hand, appears and starts to grow only above 7 T, as shown in Fig. 2(b). Magnetic field of 7 T along c is where a spin flop in the magnetization was reported.¹⁶ The magnetic field induced P can be attributed to linear ME effect for several reasons: (1) Polarizations for both directions are linearly dependent on $H_{\parallel c}$. (2) The G-type magnetic structure with spins along c belongs to $\bar{3}'$ point group which does permit a non-zero α_{zz} . (3) A dielectric anomaly appears in the vicinity of T_N .²² The switch of polarization from P_c to P_a signifies the change of the ME tensor, and therefore of the magnetic symmetry. The ME coefficient α_{xz} and α_{zz} , deduced from the slope of the P - H curve, are 4.44×10^{-6} and 5.1×10^{-5} (CGS unit), respectively. These values are about an order of magnitude smaller than those of Cr_2O_3 .^{27,28}

In the $x=0.33$ compound, the magnetic field induced polarization persists, but its behavior differs from that in undoped compound. The threshold of field $H_{\parallel c}$ for P_a disappears. Both P_c and P_a start to increase as soon as $H_{\parallel c}$ is turned on, as shown in Fig.3(a) and (b). P_a linearly increases with $H_{\parallel c}$ (Fig.3(b)), but P_c increases first then decreases to $1 \mu\text{C}/\text{m}^2$ and remains unchanged from 4 T to 7 T (Fig.3(a)). The polarizations along the two

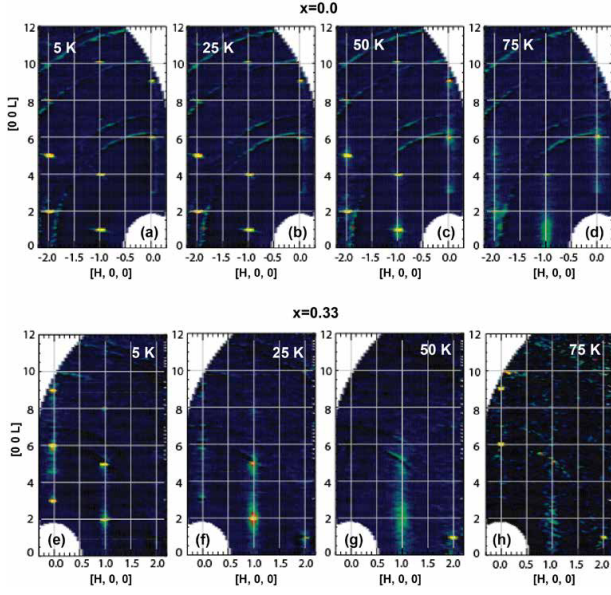


FIG. 4: (Color online) The contour plot of the diffraction pattern in the $(H,0,L)$ plane for $x=0$ at (a) 5 K, (b) 25 K, (c) 50 K, and (d) 75 K. (e)-(h) show the same plane for $x=0.33$ at 5 K, 25 K, 50 K and 75 K, respectively. The intensity scale in (h) is different from other panels to show the diminishing diffuse scattering.

different E directions also have different temperature dependence. The onset temperature of P_a is at about 20 K while that of P_c is 27 K. Moreover, at $H_{\parallel c} = 1$ T the initial increase of P_c on cooling is considerably suppressed below 20 K, as shown by the red circle in Fig.3(a). Such an anomaly is absent for higher fields. Additionally, the P_a and P_c can also be induced by $H//a$ (Fig. 3(c) and (d)), which does not give rise to any polarization in the $x=0$ compound. Compared to the $H_{\parallel c}$ -induced polarizations, the onset temperature for the polarization with a -axis field is different though. In Fig.3(c) and (d), P_c and P_a both appear below 17.5 K. Different critical values of $H_{\parallel a}$ are required for P_c and P_a , which are around 2 Tesla and 4 Tesla, respectively. Above the critical $H_{\parallel a}$, the polarization increases with the $H_{\parallel a}$ in both cases. The polarization was not observed in the $x=0.50$ and 0.68 crystals regardless of the directions and magnitudes of the applied magnetic field. The knowledge of detailed spin structures in these mixed compounds and their evolution with temperature and magnetic field is needed to understand the coupling of the ferroelectric order with the magnetic one.

B. The Ni – doping dependence of magnetic order

1. The G-type AFM phase

The structural refinements show that the 4 compositions of $\text{Mn}_{1-x}\text{Ni}_x\text{TiO}_3$ compounds all crystallize in space group $R\bar{3}$. Their ilmenite structure and the two

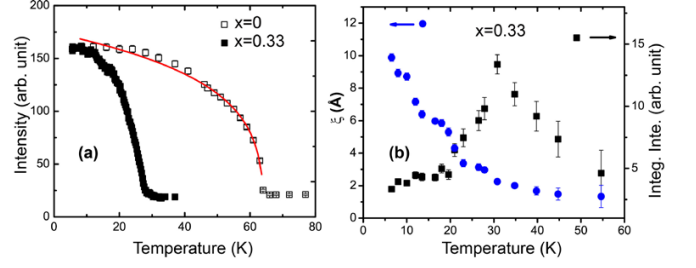


FIG. 5: (Color online) (a) The intensity of the magnetic peak (1 0 1) as a function of temperature in $x=0$ and $x=0.33$. (b) The integrated intensity of the diffuse scattering and short-range correlation length along c as a function of temperature in $x=0.33$.

generalized spin configurations are depicted in Fig.1. Along the c -axis of the hexagonal lattice, $\text{Mn}^{2+}/\text{Ni}^{2+}$ and Ti^{4+} layers alternate and every third octahedral site is vacant. The magnetic structure of MnTiO_3 is G-type where nearest inter- and intra-planar neighbor spins are antiparallel,¹⁸ which has the propagation wave vector $\vec{q}=(0,0,0)$. The magnetic peaks coincide with the allowed nuclear ones ($-H+K+L=3n$, n is integer). The contour plots of the magnetic diffraction in the $(H0L)$ scattering plane, obtained by subtracting the high temperature (140 K) data as background, are shown in Fig. 4(a-d). The temperature dependence of the (1,0,1) position gives the Néel temperature $T_N \sim 64 \pm 2.4$ K. The absence of peaks along $[0,0,L]$ implies that the Mn^{2+} moments are along c . The ridge-like diffuse scattering along c starts to develop around 90 K. Fig.4(d) show the diffuse peaks at 75 K, which center on the magnetic Bragg peak positions such as (1,0,1), instead of (1,0,0).²⁹ On cooling the diffuse scattering intensity reaches its maximum at T_N , then quickly decreases.³⁰ Before Lorentzian peaks completely disappear at 4 K, they coexist with the Gaussian line shape, suggesting the coexistence of long-range AFM order and short range 2D AFM correlations.

The spin structure of $x=0.33$ system remains G-type as suggested by the unchanged magnetic peak positions in Fig. 4(e). The onset temperature of the AFM order is suppressed by Ni-doping to 27.6 K (Fig. 5(a) and Fig. 6(a)). However, the temperature dependence of the magnetic peaks, shown in Fig.5(a) and Fig.6(a), indicates an extra phase transition at $T_R=17.5$ K. Both (0,1,2) and (1,0,1) show a kink at this temperature and (0,0,3) suddenly gains intensity below T_R suggesting the spins rotate away from the c -axis and obtain the component of the moment perpendicular to the wavevector. To accurately characterize the magnetic configuration and monitor the changing spin directions, 116 magnetic Bragg peaks were collected for every 1 K between 5 K and T_N . In the magnetic structure refinement using FullProf, three equivalent magnetic domains were taken into account, only one of which is presented here. The component of the ordered moment in the ab -plane at all measured temperatures lies in the a -direction. So the spin directions are specified by

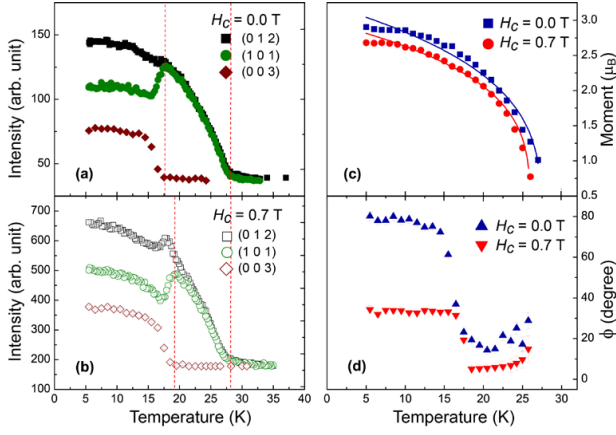


FIG. 6: (Color online) Temperature dependence of (a) various magnetic reflections of the $x=0.33$ compound without magnetic field, (b) magnetic peaks with applied external magnetic field of 0.7 T, (c) the refined ordered moment and (d) the angle ϕ between the ordered spins and c .

ϕ , the angle between the spin and the c -direction in the ac -plane, as shown in Fig.1(b). The blue up-triangles in Fig.6(d) show the spin orientation ϕ as a function of temperature. The ordered spins between T_N and T_R are close to but not quite along c ($\phi=14.26^\circ$ at 20.5 K). Cooling across T_R the spins abruptly rotate by more than 60 degrees toward a . The angle ϕ reaches 80.1° at 4 K. These results are different from the established phase diagram which shows spins lying exactly along a between T_N and T_R and exactly along c below T_R .^{19,20} Fig. 6(c) shows the refined ordered moment as a function of temperature, which is a smooth decrease and proves that the kinks of the magnetic peak intensities at 20 K in Fig. 6(a) are solely caused by the reorientation of the spins.

The diffuse scattering at this composition becomes more prevalent: The ridge along c persists to the lowest measured temperature, extends high above T_N , and becomes broader than the undoped system (Fig.4(g)). The integrated intensity of the diffuse component around (1,0,1) also reaches its maximum at T_N and decreases quickly on both sides (Fig.5(b)). In addition, the Lorentzian line width does decrease on cooling. The inter-plane spin correlation length ξ is smaller than the nearest neighbour interlayer distance above T_N , implying the short range order is basically 2-dimensional (2D). The crossover from 2D to 3D occurs close to T_N when the correlation length becomes bigger than the distance between neighbouring Mn/Ni layers. ξ does not diverge at T_N but continues to increase on cooling to the base temperature. With some short-range correlated spins participating in the establishment of 3-dimensional long range order, some remain short-ranged at low temperature.

2. Magnetic field effect on the AFM order ($x=0.33$)

The onsets of P_a and P_c occur at T_R and T_N , respectively. The anomalous suppression of P_c under low field

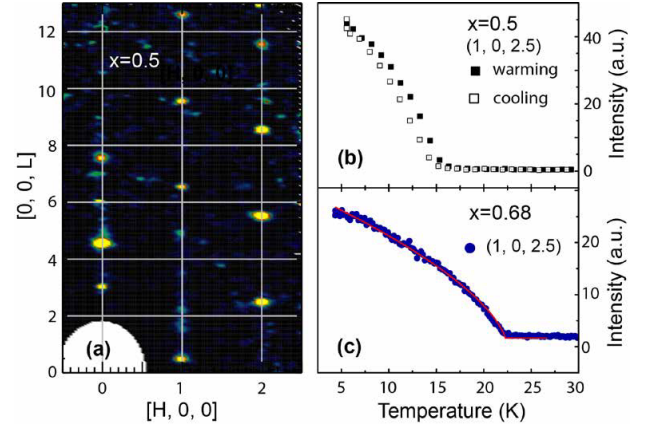


FIG. 7: (Color online) (a) Contour plot of the (H,0,L) scattering plane collected at 4 K with the 25 K data subtracted as the background. The visible (0,0,3) and (0,0,6) peaks do not show temperature dependence. The temperature dependence of the magnetic peak (1,0,2.5) for the (b) $x=0.5$ and (c) $x=0.68$ compound.

also coincides with T_R . Given that there is no detectable structural transitions at these temperatures, the electric polarization in the $x=0.33$ system apparently originates from the magnetic order. To investigate if this is linear or higher order ME effect, it is critical to know the effect of c -direction magnetic field on the symmetry of the AFM order. The same crystal was aligned and mounted in the permanent magnet set which were mounted in a CCR with the c -axis parallel to the field direction. The selected magnets provided a field of 0.7 T at the sample position, which was measured by Gauss meter. The actual angle between c and the field was determined to be 6° using the observed angle χ of the Bragg peak (0,0,6). The temperature dependence of the magnetic peak intensities is shown in Fig.6(b). Due to the geometrical restrictions imposed by the magnets, fewer magnetic peaks were accessible, but enough were collected for an unambiguous refinement of the spin structure at each temperature. The field kept the spin structure and T_N intact, but increased T_R from 17.5 K to about 20 K, making it the same as the onset temperature for P_a . The result of spin structure refinements shows that the spins were pulled toward c by the field, both below and above T_R . ϕ is reduced to about 5° above T_R and around 30° below. It is reasonable to assume that the spins would have been aligned along the c -axis had a higher field been perfectly applied along c . The spin-rotation transition is made sharper by the small field. Another effect of this field is suppressing the moment as shown in Fig. 6(c).

3. A-type AFM structure ($x=0.50$ and 0.68)

The SG state forms between $x=0.4$ and 0.48 according to the established phase diagram.^{19,23,31} The contour plot of the (H,0,L) scattering plane for $x=0.5$ is taken at 4 K with 20 K data subtracted and shows a new magnetic wave vector $\vec{q}=(0,0,1.5)$, indicating the A-type magnetic

order has taken over at this composition. There is no sign of diffuse scattering along c . The Bragg peak (1,0,2.5), shown in Fig.7(b), decreases smoothly in intensity without an abrupt transition and completely vanishes above 15 K. The smeared transition also shows hysteresis on cooling suggesting the spin glass phase still lingers at this composition. This is consistent with the magnetization measurement.³¹ The coexistence of long range AFM order with the spin glass order has been predicted³² in such a magnetically non-diluted system. Similar phenomena have been observed in $\text{Mn}_{1-x}\text{Fe}_x\text{TiO}_3$, where the dominant nearest neighbor interactions compete with each other and give rise to a strong magnetic frustration within the honeycomb layer.^{33,34} The spin structure refinement agrees with the A-type model with the spins lying along a -axis, as shown by Fig. 1(c). As the nickel content increases to 0.68, the arrangement of the ordered moments remains A-type. Both the Néel temperature and the size of the ordered magnetic moment at low temperature increase. T_N increases to 21.5 K and the transition is abrupt and first-order like, contrasting with that of the $x=0.5$ sample. The structural parameters at 4 K and the magnetic orders in compounds of different Ni concentrations are summarized in Table 1.

TABLE I: The lattice parameters, atom parameters, magnetic structures, magnetic phase transition temperatures, the ordered moments of the magnetic orders, and the R factors of the structure refinements in various $\text{Mn}_{1-x}\text{Ni}_x\text{TiO}_3$ compounds. m_a and m_c denote the projected moment on the hexagonal a - and c -axes respectively. R_{F^2} is calculated by $R_{F^2}=100 \sum_n (|G_{obs}^2 - G_{calc}^2|) / \sum_n G_{obs}^2$, where G is the structure factor and n the number of reflections used.

refined x	x=0.00 ³⁵	x=0.33	x=0.50	x=0.68	x=1.00 ³⁶
a	5.14	5.12	5.06	5.05	5.04
c	14.28	14.15	13.91	13.91	13.81
Mn_z/Ni_z	0.3600	0.347(2)	0.3471(2)	0.3509(5)	0.3509
Ti_z	0.1476	0.1504(5)	0.1466(2)	0.1426(8)	0.1450
O_x	0.3189	0.3188(6)	0.3166(2)	0.3161(8)	0.3142
O_y	0.031	0.0264(8)	0.0246(3)	0.0205(7)	0.016
O_z	0.2439	0.2449(3)	0.2459(1)	0.2458(3)	0.2465
magn.					
struc.	G-type	G-type	A-type	A-type	A-type
T_N	64	27.6	15	21.5	21.8 ¹⁸
T_R	—	17.51	—	—	—
m_a (μ_B)	0	2.86(2)	1.36(3)	2.06(3)	2.25 ¹⁸
m_c (μ_B)	4.55 ¹⁸	0.5(1)	0	0	0
Nucl. R_{F^2}		7.77	6.33	8.05	
Magn. R_{F^2}		3.97	15.2	9.6	

IV. DISCUSSION AND CONCLUSION

The ionic radius of Ni^{2+} (0.70 Å) is smaller than that of Mn^{2+} (0.80 Å), so the effect of increasing Ni^{2+} content on the nuclear structure is to be expected. As exhibited in Table 1, a and c both decrease with increasing Ni-doping, so do the z values of the atoms on 6c sites (Mn, Ni, and Ti). The value of O_y for the oxygen site, already

small in MnTiO_3 (0.031), is systematically reduced by the Ni-replacement and becomes 0.016 in NiTiO_3 . However, its minuscule value keeps the crystal from having mirror planes, so is important for the crystallographic symmetry and consequently for the magnetic symmetry. The effective moment for Mn^{2+} in MnTiO_3 , 4.55 μ_B , is smaller than the spin-only value. This can be ascribed to the incomplete ordering of Mn and Ti or the existence of Mn^{3+} .¹⁸ Both the effective moment and the Néel temperature change with Ni concentration as a result of the competing anisotropies and frustrated exchange interactions. This change is more rapid on the Mn-rich region. Both values are considerably reduced at $x=0.5$, which is compatible with the observed spin glass behavior. In the $x=0.68$ compound, the intra-layer exchange interactions among the Ni^{2+} ions become so dominant that T_N and the ordered moment are very close to those in the pure NiTiO_3 . Because of the similar radii of Ni and Ti ions, more incomplete ordering exists in NiTiO_3 ¹⁷, which is mainly responsible for the less-than-expected moment size of Ni^{2+} .¹⁸

The Mn^{2+} and Ni^{2+} ions have distinct single ion anisotropies as manifested by their different easy axes in the ilmenites^{17,18} and other compounds such as barium fluorides BaMnF_4 ³⁷ and BaNiF_4 .³⁸ The added Ni cations randomly replace Mn on the octahedral sites and weaken the spin correlations, more so in the inter-planar direction, as indicated by the enhanced diffuse scattering in the $x=0.33$ system. Although the spin correlation starts to form high above T_N , the electric polarization does not occur until the long range G-type magnetic order is established. When the spins are parallel to the c -axis, the magnetic group symmetry is $R\bar{3}'$ and the point symmetry is $\bar{3}'$. As the collinear AFM moments tilt away from the c axis, the emerged a -axis components in the hexagonal layer loses the 3-fold rotation symmetry. The magnetic space group then becomes $P\bar{1}$ and the magnetic point symmetry becomes $\bar{1}'$. Since the nonzero O_y value keeps the crystal from having 2-fold rotation axis and mirror planes. Even if the spins completely lie in the a -axis, the point group of the magnetic symmetry is not $2'/m$ as it appears to be. The restrictions from the non-magnetic anion sites must be obeyed as the Neumann's principle requires the physical property tensor be invariant under all the permissible operations of the crystallographic symmetry^{39,40}.

This observation is the key to understand the observed electric polarizations summarized in Fig.2 and Fig.3 for $x=0$ and 0.33, respectively. Both $\bar{3}'$ and $\bar{1}'$ are among the 58 magnetic point groups that have non-zero elements in their ME susceptibility tensors.⁸ The former has both diagonal $\alpha_{xx}=\alpha_{yy}$, α_{zz} and off-diagonal components $\alpha_{xy}=-\alpha_{yx}$, while the latter does not impose any restrictions on the form of ME tensor and all tensor components are non-zero. The G-type structure with c -axis spins ($\phi=0$) in MnTiO_3 , permits α_{zz} as indeed observed. In the $x=0.33$ system, the spins tilt away from c while maintaining the G-type structure and lowers the symmetry to

$\bar{1}'$. The symmetry remains as $\bar{1}'$ even for $T_R < T < T_N$ unless a c -direction magnetic field pull the spins back along c (Fig. 6(d)), which enables the recovery of the $\bar{3}'$ symmetry in this temperature range. This explains why α_{zz} , allowed by both symmetries, exist in the entire $T < T_N$ range. Cooling across T_R at 20 K, $\bar{1}'$ arising from the collinear spin rotation triggers α_{xz} , which is prohibited by $\bar{3}'$. At the same temperature, α_{zz} exhibits considerable suppression due to the reduced c -component of the moment, as shown by the red triangle in Fig.6(d). The change of magnetic point symmetry satisfactorily explains the temperature dependence of the observed P_a and P_c . It is clear that coupling of the ferroelectric order and magnetic order is due to the linear ME effect. The case of $x=0.33$ system is different from a normal linear ME effect, as in $x=0$, in that the spin directions vary with external magnetic field, which fails the linear dependence of the polarization on magnetic field.

With the ties between the two orders established, one can use the polarization to predict the spin structures at higher fields, as they are difficult to determine experimentally. The representation analysis using SARAH program⁴¹ shows that for the space group $R\bar{3}$ with magnetic propagation vector $\mathbf{k}=(0,0,0)$, the G-type is the only possible AFM spin arrangement. So if one assumes the magnetic wave vector remains unchanged, ϕ alone should be sufficient to describe all the spin structures under moderate magnetic field. With higher $H_{\parallel c}$ in the $x=0.33$ compound, ϕ remains different in the two temperature regions. The fact that P_a only exists below T_R (Fig.2(d)) suggests that up to $H_{\parallel c}=7$ T, $\phi=0$ for $T_R < T < T_N$ and that $\phi \neq 0$ for $T < T_R$. As the magnetic field is applied along a , the observed α_{xz} (Fig.3(d)), prohibited by $\bar{3}'$, suggests the $\bar{1}'$ magnetic point symmetry.

The electric polarization flop has been observed in a few multiferroic materials, including rare-earth manganites RMnO_3 ,^{42,43} RMn_2O_5 ⁴⁴ and the mineral h  bnerite MnWO_4 ,⁴⁵ which generally have incommensurate non-collinear spiral spin structures. In these materials the P -flop is typically caused by the flop of spiral or cycloid plane. MnTiO_3 is a rare case of magnetic field induced P -flop with a collinear magnetic structure. In the $x=0.33$ system, the polarizations in the two directions are turned on by the same field and coexist for $T < T_R$, so this is not a typical P -flop. But the reciprocal interactions between P_a and P_c and their different on-set temperatures makes it a unique type of ME control. The Co-doped MnWO_4 is another case of P -flop caused by the com-

peting single ion anisotropies, which is achieved by the flop of the spin helix.^{46,47} But the magnetic frustration and complex magnetic structure make this type of control difficult to repeat in other compounds in terms of materials design. In comparison, the collinear spin rotation in $\text{Mn}_{1-x}\text{Ni}_x\text{TiO}_3$ can be easily created for a random mixture of two antiferromagnets with orthogonal easy axes. A new intermediate phase whose easy axis tilts oblique to the easy axes of the pure systems, and two second order transitions are all predicted by mean field approximation.^{48,49} Such predictions have also been fulfilled in other random mixtures such as $\text{K}_2\text{Mn}_{1-x}\text{Fe}_x\text{F}_4$ ⁵⁰ and $\text{Co}_{1-x}\text{Fe}_x\text{Cl}_2\text{H}_2\text{O}$.⁵¹

V. SUMMARY

The structural, magnetic and electric properties have been studied for 4 typical compositions of $\text{Mn}_{1-x}\text{Ni}_x\text{TiO}_3$. Magnetic field induced electric polarizations have been observed in the compositions $x=0$ and 0.33, both of which have the G-type magnetic order. In the $x=0$ system, the polarization flops from P_c to P_a as the spin flop transition is triggered at $H_{\parallel c}=7$ T. In $x=0.33$, P_a is turned on together with P_c by $H_{\parallel c}$. Additionally, P_a and P_c can also be induced by $H_{\parallel a}$. By studying the magnetic structure and phase transition with and without magnetic field, the occurrence of the new ME coupling is attributed to the emergent point group symmetry as the antiferromagnetically coupled spins tilt collinearly toward the a -axis. Such spin rotation results from the strong competition of single ion anisotropy of the transition metal elements and provides a new way to tune electric polarizations. The magnetic structure of the $x=0.5$ and 0.68 systems is the same as that of the NiTiO_3 . No polarization was observed.

V. ACKNOWLEDGMENTS

The research at Oak Ridge National Laboratory's High Flux Isotope Reactor was sponsored by the Scientific User Facilities, Office of Basic Energy Sciences, US Department of Energy. The authors are grateful for fruitful discussions with Bryan C. Chakoumakos. H.D.Z thanks for the support from JDRD program of University of Tennessee. NHMFL is supported by National Science Foundation (DMR-0654118), the State of Florida, and the U.S. Department of Energy.

¹ M. Fiebig, Journal of Physics D:Applied Physics **38**, R123 (2005).

² S.-W. Cheong and M. Mostovoy, Nature Materials **6**, 13 (2007).

³ W. Eerenstein, N. D. Mathur, and J. F. Scott, Nature **442**, 759 (2006).

⁴ D. I. Khomskii, Journal of Magnetism and Magnetic Ma-

terials **306**, 1 (2006).

⁵ W. Kleemann, P. Borisov, S. Bedanta, and V. V. Shvartsman, Ieee Transactions on Ultrasonics Ferroelectrics and Frequency Control **57** (2010).

⁶ T. Kimura, Annual Review of Condensed Matter Physics, Vol 3 **3**, 93 (2012).

⁷ A. Agyei and J. L. Birman, J. Phys:Condens. Matter **2**,

- 3007 (1990).
- ⁸ J.-P. Rivera, *European Physical Journal B* **71**, 299 (2009).
 - ⁹ A. B. Harris, *Physical Review B* **76**, 054447 (2007).
 - ¹⁰ A. K. Zvezdin and A. P. Pyatakov, *Low Temperature Physics* **36**, 532 (2010).
 - ¹¹ E. Bousquet and N. Spaldin, *Physical Review Letters* **107**, 197603 (2011).
 - ¹² M. Mostovoy, A. Scaramucci, N. A. Spaldin, and K. T. Delaney, *Physical Review Letters* **105**, 087202 (2010).
 - ¹³ E. Bousquet, N. A. Spaldin, and K. T. Delaney, *Physical Review Letters* **106**, 107202 (2011).
 - ¹⁴ R. M. Hornreich and S. Shtrikman, *Phys. Rev.* **161**, 506 (1967).
 - ¹⁵ J. C. Wojdeł and J. Íñiguez, *Physical Review Letters* **103**, 267205 (2009).
 - ¹⁶ H. Yamauchi, H. Hiroyoshi, M. Yamada, H. Watanabe, and H. Takei, *Journal of Magnetism and Magnetic Materials* **31-4**, 1071 (1983).
 - ¹⁷ Y. Ishikawa and S. Akimoto, *Journal of Physical Society of Japan* **13**, 1298 (1958).
 - ¹⁸ G. Shirane, S. J. Pickart, and Y. Ishikawa, *Journal of the Physical Society of Japan* **14**, 1352 (1959).
 - ¹⁹ H. Yoshizawa, H. Kawano, H. Mori, S. Mitsuda, and A. Ito, *Physica B* **180**, 94 (1992).
 - ²⁰ A. Ito, H. Kawano, H. Yoshizawa, and K. Motoya, *Journal of Magnetism and Magnetic Materials* **104**, 1637 (1992), part 3 International conf on magnetism Sep 02-06, 1991 Edinburgh, scotland.
 - ²¹ H. Kawano, H. Yoshizawa, A. Ito, and K. Motoya, *Journal of the Physical Society of Japan* **62**, 2575 (1993).
 - ²² N. Mufti, G. R. Blake, M. Mostovoy, S. Riyadi, A. A. Nugroho, and T. T. M. Palstra, *Physical Review B* **83** (2011).
 - ²³ Y. Yamaguchi, T. Nakano, Y. Nozue, and T. Kimura, *Physical Review Letters* **108** (2012).
 - ²⁴ R. E. Cohen, *Nature* **358**, 136 (1992).
 - ²⁵ X. H. Deng, W. Lu, H. Wang, H. T. Huang, and J. Y. Dai, *Journal of Materials Research* **27**, 1421 (2012).
 - ²⁶ J. Rodriguez-Carvajal, *Physica B* **192**, 55 (1993).
 - ²⁷ Y. F. Popov, A. M. Kadomtseva, D. V. Belov, G. P. Vorob'ev, and A. K. Zvezdin, *Jetp Letters* **69**, 330 (1999).
 - ²⁸ J.-P. Rivera, *Ferroelectrics* **161**, 165 (1994).
 - ²⁹ J. Akimitsu and Y. Ishikawa, *Journal of the Physical Society of Japan* **42**, 462 (1977).
 - ³⁰ J. Akimitsu, Y. Ishikawa, and Y. Endoh, *Solid State Communications* **8**, 87 (1970).
 - ³¹ A. Ito, H. Aruga, E. Torikai, M. Kikuchi, Y. Syono, and H. Takei, *Physical Review Letters* **57**, 483 (1986).
 - ³² D. Sherrington and S. Kirkpatrick, *Physical Review Letters* **35**, 1792 (1975).
 - ³³ H. Yoshizawa, S. Mitsuda, H. Aruga, and A. Ito, *Physical Review Letters* **59**, 2364 (1987).
 - ³⁴ H. A. Katori and A. Ito, *Journal of the Physical Society of Japan* **62**, 4488 (1993).
 - ³⁵ K. Kidoh, K. Tanaka, F. Marumo, and H. Takei, *Acta Crystallographica Section B-Structural Science* **40**, 329 (1984).
 - ³⁶ H. Boysen, F. Frey, M. Lerch, and T. Vogt, *Zeitschrift Fur Kristallographie* **210**, 328 (1995).
 - ³⁷ A. Poole, B. Roessli, O. Zaharko, and K. W. Krämer, *Journal of Physics: Condensed Matter* **23**, 266004 (2011).
 - ³⁸ D. E. Cox, M. Eibschütz, H. J. Guggenheim, and L. Holmes, *Journal of Applied Physics* **41**, 943 (1970).
 - ³⁹ R. R. Birss, *Symmetry and magnetism* (North-Holland, 1964), chap. 4.
 - ⁴⁰ S. Bhagavantam and P. V. Pantulu, *Proceedings of the Indian Academy of Sciences* **59**, 1 (1964).
 - ⁴¹ A. Wills, *Physica B* **276**, 680 (2000).
 - ⁴² T. Kimura, T. Goto, H. Shintani, K. Ishizaka, T. Arima, and Y. Tokura, *Nature (London)* **426**, 55 (2003).
 - ⁴³ J. Strempfer, B. Bohnenbuck, M. Mostovoy, N. Aliouane, D. N. Argyriou, F. Schrettle, J. Hemberger, A. Krimmel, and M. von Zimmermann, *Physical Review B* **75** (2007).
 - ⁴⁴ M. Fukunaga, Y. Sakamoto, H. Kimura, Y. Nada, N. Abe, K. Tanigushi, T. Arima, S. Wakimoto, M. Takeda, K. Kakurai, et al., *Physical Review Letters* **103**, 077204 (2009).
 - ⁴⁵ K. Tanigushi, N. Abe, T. Takenobu, Y. Isawa, and T. Arima, *Physical Review Letters* **97**, 097203 (2006).
 - ⁴⁶ K. C. Liang, Y. Q. Wang, Y. Y. Sun, B. Lorenz, F. Ye, J. A. Fernandez-Baca, H. A. Mook, and C. W. Chu, *New Journal of Physics* **14**, 073028 (2012).
 - ⁴⁷ F. Ye, S. Chi, J. A. Fernandez-Baca, H. Cao, K. C. Liang, Y. Wang, B. Lorenz, and C. W. Chu, *Physical Review B* **86**, 094429 (2012).
 - ⁴⁸ F. Matsubara and S. Inawashiro, *Journal of Physical Society of Japan* **42**, 1529 (1977).
 - ⁴⁹ T. Oguchi and T. Ishikawa, *Journal of Physical Society of Japan* **45**, 1529 (1978).
 - ⁵⁰ L. Bevaart, E. Frikkee, J. V. Lebesque, and L. J. de Jongh, *Solid State Communications* **25**, 539 (1978).
 - ⁵¹ K. Kobayashi and K. Katsumata, *Journal of Physical Society of Japan* **45**, 697 (1978).